Spatial Filtering using Pinholes at COAST

D. St-Jacques, J. E. Baldwin, R. C. Boysen, C. A. Haniff,
P. R. Lawson[a], J. Rogers, P. J. Warner, D. M. A. Wilson and J. S. Young

Mullard Radio Astronomy Observatory, Cavendish Laboratory,
Madingley Road, Cambridge, CB3 0HE, UK

[a]Now at: Jet Propulsion Laboratory, 4800 Oak Grove Drive,
Pasadena, CA 91109, USA

ABSTRACT

Visibility measurements obtained with optical astronomical interferometers are corrupted by random wavefront distortions of atmospheric origin. In this paper we discuss how spatial filtering using pinholes can lead to increased measured visibility, improved signal-to-noise ratio and reduced dependence on seeing fluctuations. The potential for calibrating visibility measurements without resorting to a separate calibrator target is also discussed. Results of preliminary pinhole experiments carried out with the Cambridge Optical Aperture Synthesis Telescope are presented.

Keywords: COAST, interferometry, atmospheric seeing, spatial filtering, pinhole, visibility calibration

1. INTRODUCTION

In this paper we discuss the potential benefits of using pinholes as spatial filters in the light paths of astronomical optical interferometers, with the aim of countering the deleterious effects of atmospheric turbulence. The study is applied more particularly to the Cambridge Optical Aperture Synthesis Telescope (COAST).

Picture the incoming starlight as a continuous flow of wavefronts. The principal effect of their travelling through atmospheric turbulence is the impression of random and rapidly changing phase perturbations upon them; there is also a certain level of scintillation, or intensity perturbation involved. In other words, by the time it reaches the ground, starlight has lost some of its spatial coherence. Consequently, when light beams collected at separate telescopes are combined in an interferometric fashion, the loss of coherence translates into a loss in fringe visibility. This is due to the general disagreement between various parts of the individual beams as to what the overall phase and intensity relationships are at any given time. A reduced and constantly changing "compromise" visibility is thus measured.

Spatial filtering using pinholes is a simple and rugged way of improving a beam's spatial coherence. The technique is used routinely with laser light in areas such as holography and optical data processing. Figure 1 shows a schematic of a spatial filtering set-up and how this cleans a corrupted wavefront. The corrupted wavefront can be thought of as the sum of a flat, "clean" component and a random noise component. When the first lens focuses the beam, it effectively performs a Fourier Transform[1] ($\mathcal{FT}$). The flat component becomes a sharp peak, and the random noise component becomes an extended halo. The pinhole located at the focus of the first lens acts as a low-pass filter, letting through most of the "good" light from the peak, and blocking most of the "bad" halo light. Downstream of the second lens, the wavefront has lost some of its brightness, but retrieved most of its coherence.

We will review formally the nature of the atmospheric coherence losses, and see how spatial filtering using pinholes can partly alleviate two ensuing problems:

- in photon-limited conditions, coherence losses result in impoverished signal-to-noise ratio (SNR) when measuring fringe visibility or phase. This is of particular concern for imaging arrays such as COAST, when intrinsically weak and asymmetric image components are measured;
- the magnitude of the coherence loss is dependent on the statistical properties of the turbulence at the exact moment the measurement is made, and this leads to dire calibration problems.

We will conclude by presenting results of preliminary pinhole experiments carried out at COAST.

Send correspondence to D. St-J.
E-mail: dsj@mrao.cam.ac.uk

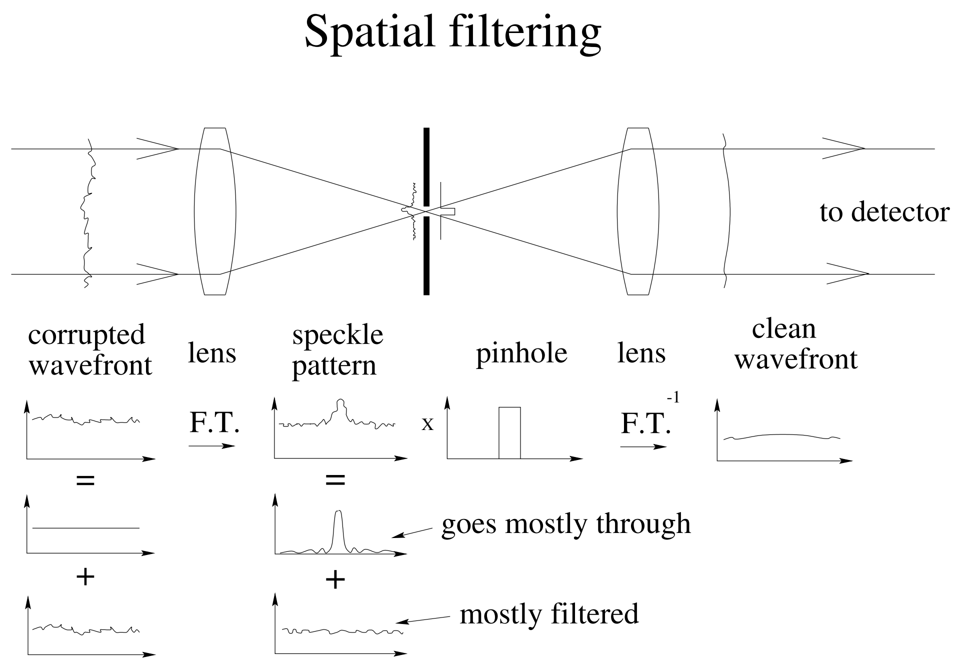

Figure 1. Spatial filter set-up showing how a corrupted incoming wavefront is cleaned of its random noise component.

2. COAST VISIBILITY MEASUREMENTS

In the simplest type of visibility measurement made at COAST, two separate telescopes track the same source and send the collected light back to the central laboratory, collimated and beam-reduced. A fast guiding mirror, controlled by a closed-loop acquisition system compensates for any source wander of atmospheric origin, hence maintaining the beams' alignment. The appropriate amount of optical path delay (OPD) is continuously added to one beam to compensate for the motion of the source across the sky. A rapid triangular sawtooth oscillation is added to this smooth tracking motion, scanning back and forth through the nominal zero OPD position. The sawtooth amplitude is such that all the fringes made available by the optical bandwidth are scanned. The sawtooth period is tuned to the seeing conditions such that the corresponding fringe frequency is comfortably higher than most frequencies associated with the signal scintillation of atmospheric origin. The two beams are then superimposed using a beamsplitter plate and focused together onto a detector, read out fast enough to effectively freeze turbulence and provide adequate fringe sampling. An iris located just before the detector lens determines the pupil of the system. This is also where a narrow band filter sets the observation wavelength and bandwidth.

Consider the limiting case of a monochromatic observation at wavelength λ. Let $\psi_1(\vec{r},t)$ and $\psi_2(\vec{r},t)$ represent the scalar electric field associated with each beam at time t in the pupil $\vec{r}$–plane. If the iris size corresponds to an equivalent telescope diameter D, let the system pupil be defined by

$$P(\vec{r}) = \begin{cases} 1 & \text{for } |\vec{r}| \leqslant D/2 \\ 0 & \text{otherwise} \end{cases} \tag{1}$$

$\psi_1(\vec{r},t)$ and $\psi_2(\vec{r},t)$ are complex quantities, randomly corrupted both in amplitude and phase by atmospheric turbulence. Assuming the detector lens is perfect, the (complex) electric fields $A_1(\vec{\alpha},t)$ and $A_2(\vec{\alpha},t)$ corresponding to each beam in the detector $\vec{\alpha}$–plane are given by a Fourier transform relation:

$$A_i(\vec{\alpha},t) = \mathcal{FT}\{\ P(\vec{r})\ \psi_i(\vec{r},t)\ \}, \quad i = 1,2. \tag{2}$$

If $\delta(t)$ is the sawtooth OPD imposed on one of beams, say beam 2, the intensity signal read out at time t is obtained by integrating the square of the sum of the two electric fields at each point on the detector plane:

$$I(t) = \iint_{\vec{\alpha}} \left| A_1(\vec{\alpha},t) + A_2(\vec{\alpha},t)\ e^{i2\pi\delta(t)/\lambda} \right|^2\ d^2\vec{\alpha}. \tag{3}$$

Expanding the square, the detected intensity can be rewritten as

$$I(t) = I_1(t) + I_2(t) + |B_{12}(t)| \cos\left(2\pi\delta(t)/\lambda + b_{12}(t)\right), \tag{4}$$

where B_{12} is the instantaneous complex fringe modulation depth:

$$\begin{aligned} B_{12}(t) &= |B_{12}(t)|\, e^{ib_{12}(t)} \\ &= 2 \iint_{\vec{\alpha}} A_1^*(\vec{\alpha}, t)\, A_2(\vec{\alpha}, t)\, d^2\vec{\alpha}, \end{aligned} \tag{5}$$

and I_1, I_2 are the intensities one would measure from either arms on their own:

$$I_i(t) = \iint_{\vec{\alpha}} |A_i(\vec{\alpha}, t)|^2\, d^2\vec{\alpha}, \quad i = 1, 2. \tag{6}$$

Normally, in an attempt to collect all the available light, the stellar image is made small compared to the detector area; this is equivalent to saying integrals 5 and 6 are indeed performed over the entire $\vec{\alpha}$–plane.

The data stream is split into sections corresponding to individual ramps of the sawtooth OPD scan, which are individually Fourier transformed and squared. From the average of these individual power spectra one can recover $\langle |B_{12}|^2 \rangle$, the squared fringe modulation depth averaged through the whole data set. This will unambiguously appear as the amount of signal power under a peak at the fringe frequency set by the ratio of the sawtooth rate of scan and the observation wavelength. This peak is broadened by the random atmospheric modulation of the OPD but well separated from the low-frequency atmospheric scintillation. See the separate paper by John Baldwin[2] for examples of such spectra. Dividing by the square of the average intensity, we form the following squared visibility estimator:

$$\widehat{\mathrm{V}^2} = \frac{\langle |B_{12}|^2 \rangle}{\langle I_1 + I_2 \rangle^2}, \tag{7}$$

where the angle brackets denote ensemble averaging. In practice, an additional factor is required to account for the non-zero filter bandwidth and the resulting fringe envelope. Note that the contribution of a particular fringe realization to the estimator is in proportion to its modulation depth, not its visibility.

$\widehat{\mathrm{V}^2}$ is less than the intrinsic object squared visibility $\mathrm{V}^2_{\mathrm{true}}$. Phenomenologically, apart form the bandwidth factor, it is reduced by more or less fixed coherence losses η^2_{inst} of instrumental origin, mainly due to optical surfaces and guiding error, and by random coherence losses η^2_{atm} due to atmospheric turbulence:

$$\widehat{\mathrm{V}^2} = \mathrm{V}^2_{\mathrm{true}}\, \eta^2_{\mathrm{inst}}\, \eta^2_{\mathrm{atm}}. \tag{8}$$

At COAST, the product $\eta^2_{\mathrm{inst}}\ \eta^2_{\mathrm{atm}}$ is normally calibrated out by dividing $\widehat{\mathrm{V}^2}$ by the result of a contemporaneous measurement made on a nearby calibrator star of unit or otherwise known visibility. The unpredictable variations in the seeing conditions during the change-over time between the source and calibrator often dominate the final error on visibility measurements, at least in high light level conditions. We shall see in section 6 how spatial filtering using pinholes reduces the sensitivity to seeing fluctuations, and could even make calibrator measurements unnecessary.

At low light levels the situation is different. We see that the effect of atmospheric coherence losses is to reduce $|B_{12}|$; essentially one measures fringes of reduced amplitude sitting on top of an unaffected mean light level $\langle I_1 + I_2 \rangle$, hence the reduced visibility. But it is the mean light level which determines the photon noise in the estimation of $\widehat{\mathrm{V}^2}$ from the signal power spectrum. Noting that in power spectra the signal is squared, the SNR of $\widehat{\mathrm{V}^2}$ measurements is defined as

$$\mathrm{SNR}_{\mathrm{V}^2} = \frac{\langle |B_{12}|^2 \rangle}{\sqrt{\langle I_1 + I_2 \rangle^2}} \tag{9}$$

The delicate measurement of the fringe phase is a separate matter. Without entering into details, this is performed by fitting theoretical fringes to the raw data. Phase measurements are almost always photon-limited, and here again the signal is the reduced modulation depth while the photon noise is dictated by the mean light level. For closure phase imaging,[3] the SNR of phase measurements can be shown to be $\mathrm{SNR}_{\mathrm{V}^2}^{3/2}$.

We will see in the next section how spatial filtering can help reduce photon noise by cutting down on the mean light level without sacrificing fringe modulation too much. Because of atmospheric coherence losses a fraction of the noise-yielding mean light level is not accompanied by fringe modulation anymore, and could be done without. A parallel can be drawn with the principle of nulling imaging of dim planets around bright stars; tracking on the star, one adds half a wavelength of OPD, minimising the illumination arising from the star. This cuts down the total photon noise, while preserving the signal from the dim off-axis dim planet.

Coming back to our pinholes and referring to figure 1, the "good" image core light, corresponding to the coherent flat wavefront component, is the one yielding the fringe modulation. The "bad" halo light is the one which is not accompanied by modulation. Getting rid of this unnecessary, incoherent background illumination is the primary aim of spatial filtering.

3. ATMOSPHERIC COHERENCE LOSSES

We now derive formal statements on the effect of atmospheric turbulence on $\widehat{\mathrm{V}^2}$, and on the role of spatial filtering. For monochromatic observations, if we assume that a calibrator star of unit visibility is observed, and if we neglect instrumental imperfections, equation 7 becomes simply $\widehat{\mathrm{V}^2} = \eta_{\mathrm{atm}}^2$. From now on we will drop the "atm" subscript and refer to atmospheric coherence losses simply as η. Using the definition of B_{12} in equation 5, we can rewrite the numerator of equation 7 as

$$\begin{aligned}\langle |B_{12}|^2 \rangle &= \left\langle 2 \iint_{\vec{\alpha}} A_1^*(\vec{\alpha}) A_2(\vec{\alpha})\ d^2\vec{\alpha} \times 2 \iint_{\vec{\alpha}'} A_1(\vec{\alpha}') A_2^*(\vec{\alpha}')\ d^2\vec{\alpha}' \right\rangle \\ &= 4 \iint_{\vec{\alpha}} \iint_{\vec{\alpha}'} \langle A_1^*(\vec{\alpha}) A_1(\vec{\alpha}') \rangle \ \langle A_2(\vec{\alpha}) A_2^*(\vec{\alpha}') \rangle \ d^2\vec{\alpha}\ d^2\vec{\alpha}',\end{aligned} \tag{10}$$

where the average of the product of the integrands has been split into a product of averages of quantities related to individual telescopes. This implies statistical independence of the atmospheric perturbations over each telescope, and is justified by the assumption that the interferometer baseline is much greater than the outer scale of turbulence.[4] The quantities in brackets are referred to as image coherence functions

$$\Gamma_A(\vec{\alpha}, \vec{\alpha}') = \langle\ A^*(\vec{\alpha})\ A(\vec{\alpha}')\ \rangle, \tag{11}$$

and assuming the statistics of turbulence are the same over each telescope, equation 10 can be rewritten

$$\langle |B_{12}|^2 \rangle = 4 \iint_{\vec{\alpha}} \iint_{\vec{\alpha}'} |\Gamma_A(\vec{\alpha}, \vec{\alpha}')|^2\ \ d^2\vec{\alpha}\ d^2\vec{\alpha}'. \tag{12}$$

The better the seeing conditions, the sharper the image, and therefore the narrower and taller Γ_A is. Similarly, the denominator of equation 7 can be expressed in terms of Γ_A by taking twice the average of equation 6:

$$\langle I_1 + I_2 \rangle = \langle I \rangle = 2 \iint_{\vec{\alpha}} \Gamma_A(\vec{\alpha}, \vec{\alpha})\ d^2\vec{\alpha}. \tag{13}$$

Note that the denominator of equation 7 is the square of this expression. From now on we will refer to the mean light level as $\langle I \rangle$.

We now seek an explicit form for Γ_A in terms of seeing conditions and telescope size. Using equation 2, Γ_A can be rewritten as a four-dimensional Fourier Transform

$$|\Gamma_A(\vec{\alpha}, \vec{\alpha}')|^2 = |\mathcal{FT}\{\ P(\vec{r})\ P(\vec{r}\,')\ \Gamma_\psi(\vec{r}, \vec{r}\,')\ \}|^2, \tag{14}$$

where we have introduced the pupil $\vec{r}$–plane wavefront coherence function

$$\Gamma_\psi(\vec{r}, \vec{r}\,') = \langle\ \psi^*(\vec{r})\ \psi(\vec{r}\,')\ \rangle. \tag{15}$$

Γ_ψ describes the spatial coherence of the beams before they are focused by the detector lens.

At the pupil of a circular telescopes of diameter D, an expression for Γ_ψ in terms of Fried's seeing parameter[5] r_0 can be obtained from the adaptive optics (AO) legacy[6]:

$$\Gamma_\psi(\vec{r}, \vec{r}\,') = e^{-3.44\,\left(|\vec{r}-\vec{r}\,'|/r_0\right)^{5/3}\left(1-\mu\left(|\vec{r}-\vec{r}\,'|/D\right)^{1/3}\right)}, \tag{16}$$

where the parameter μ depends on the level of fast guiding provided by the star tracking system. This system removes any source quiver of atmospheric origin; it is also called tilt correction system because if one considers the incoming light as a series of wavefronts, then atmospheric quivering can be seen as the average wavefront tilt across the telescope aperture. At COAST we measure the tilt by measuring the centroid of the star image formed at the focus of a lens; this can be shown to be equivalent to measuring the average phase slope across the telescope aperture[7]; the expert will notice that this is different form the Zernike tilt.[8] If the tilt correction system works perfectly, i.e. if the mean slope component of the wavefront is removed at every instant, it has been shown by one of the authors (*D. St-J., PhD thesis, in preparation*) that $\mu \simeq 0.97$. If tilt correction is absent, then $\mu = 0$.

The pupil plane coherence function Γ_ψ propagates unmodified[9] through the interferometer and is the one we can use to describe the statistics of the wavefront at the aperture of the imaging lens. The image coherence function Γ_A is then seen from equation 14 to be a function of the seeing conditions r_0 and telescope diameter D.

4. SPATIAL FILTERING USING A PINHOLE

Where should the spatial filter be placed? It doesn't matter, because it doesn't matter where the "bad" photons are screened out. The filter can be placed after combination, filtering both beams at the same time. This was first tried with the Mark III interferometer, using single mode optical fibres as spatial filters.[10] This scheme is now implemented on the Palomar testbed interferometer; refer to the presentation given by J. K. Wallace during this conference for more details.[11] On the other hand, filtering can be done before beam combination, with one filter in each beams; the main reason why one would want to do this is to be able to monitor in real-time the amount of light going through each arm, which allows for direct visibility calibration if the signal is strong enough. Such a scheme has been successfully implemented with the IOTA interferometer, also using single mode optical fibres.[12] V. Coudé du Foresto presented a paper on the subject during this conference.[13]

Better still, rather than inserting the set-up of figure 1 after combination but just before the detector lens, it suffices to simply adapt the detector size (or the detector lens' focal length F) such that it only picks-up the bright image core. Formally, this means restricting the $\vec{\alpha}$-integration in equations 12 and 13 to the clear pinhole aperture:

$$\langle |B_{12}|^2 \rangle = 4 \iint\limits_{\vec{\alpha}} \iint\limits_{\vec{\alpha}'} G(\vec{\alpha})\; G(\vec{\alpha}')\; |\Gamma_A(\vec{\alpha}, \vec{\alpha}')|^2\; d^2\vec{\alpha}\; d^2\vec{\alpha}', \tag{17}$$

and

$$\langle I \rangle = 2 \iint\limits_{\vec{\alpha}} G(\vec{\alpha})\; \Gamma_A(\vec{\alpha}, \vec{\alpha})\; d^2\vec{\alpha}, \tag{18}$$

where G is the transfer function for a pinhole of diameter d

$$G(\vec{\alpha}) = \begin{cases} 1 & \text{for } |\vec{\alpha}| \leqslant d/2F \\ 0 & \text{otherwise} \end{cases} \tag{19}$$

Ideally, one would like to minimise the noise-yielding illumination $\langle I \rangle$ without sacrificing the signal modulation depth $\langle |B_{12}|^2 \rangle$. This increases the measured visibility by improving on the atmospheric coherence loss

$$\eta^2 = \frac{\langle |B_{12}|^2 \rangle}{\langle I \rangle^2} \tag{20}$$

and improves the photon-limited measurement SNR by reducing the photon noise present in the signal power spectra. From equation 9 and using equation 20, we get

$$\mathrm{SNR}_{\mathrm{V}^2} = \eta^2\; \langle I \rangle. \tag{21}$$

5. NUMERICAL RESULTS

We have used the methodology developed by Prasad[14] to solve numerically the integral equations 17 and 18, in order to evaluate the filtered coherence loss factor η^2 and the SNR of photon-limited visibility measurements $\mathrm{SNR}_{\mathrm{V}^2}$ from equations 20 and 21. The reader interested in the mathematical details should refer to Prasad's very complete work. It is worth mentioning that the integrations are actually performed in the pupil $\vec{r}$–plane, not the image $\vec{\alpha}$–plane as we've presented so far.

The calculations were performed for a range of value of two dimensionless parameters:

- D/r_0, which compares the telescope pupil size D to the turbulence strength indicator r_0. This parameter is used to compare the effect of varying seeing conditions, given a particular telescope size.
- $dD/\lambda F$, which compares the pinhole size d to the size of the Airy disc $\lambda F/D$ obtained when the detector lens of focal length F images the telescope pupil of size D in the detector image $\vec{\alpha}$–plane, in the absence of turbulence. This parameter is used to compare various combinations of pinhole and pupil sizes. For example, if this parameter equals $2 \times 1.22 = 2.44$, then the pinhole diameter just encloses the first null of the diffraction-limited Airy disc.

Figure 2 shows the computed photon-limited SNR of the measurement of visibility squared, $\mathrm{SNR}_{\mathrm{V}^2}$. The horizontal axis reads the value of the pinhole/pupil combination parameter $dD/\lambda F$, ranging from 0.5 (pinhole much smaller than the Airy disc) to 5 (pinhole much larger than the Airy disc). The vertical axis reads the value of the normalised pupil parameter D/r_0. When evaluating equation 16, perfect tilt correction has been assumed ($\mu = 0.97$). $\mathrm{SNR}_{\mathrm{V}^2}$ is a dimensionless number, but its value depends on the mean illumination; the results are given per photon, per $\pi r_0^2/4$ unit of telescope pupil area. The photon-limited $\mathrm{SNR}_{\mathrm{V}^2}$ is seen to reach a maximum for pinhole/pupil combination for which $dD/\lambda F \simeq 2$, i.e. for a pinhole a bit smaller than the pupil's diffraction limited Airy disc, and a pupil size $D \simeq 3.2 r_0$.

The nature of this result should not be surprising. Firstly, the well-known[15] no pinhole ($dD/\lambda F \to \infty$) limit plotted on figure 3 shows that even without using a pinhole, pupils of that sort of size are optimum. Note that the curves for perfect tilt-correction and no tilt correction are shown. It turns out one can afford a slightly larger aperture, as can be seen by comparing the position of the maximum on figure 4 which shows a vertical slice through figure 2 for $dD/\lambda F = 2$, which we will now refer to as the optimum pinhole size. Why is $dD/\lambda F = 2$ the optimum? This corresponds to a pinhole slightly smaller than the Airy disc, i.e. roughly the size of a speckle in the image plane, and speckles are essentially coherent regions of the image. For the size of telescopes we use at COAST, there is generally just one bright speckle present; our theoretical perfect guiding essentially ensures this central speckle remains centred on the pinhole aperture, and anything outside it we can safely mask out.

Figure 5 shows the computed coherence loss factor η as a function of the normalised pupil size D/r_0, assuming a pinhole of optimum size $dD/\lambda F = 2$ is used and tilt correction is perfect. For comparison, the well-known results for no pinhole[16] ($d \to \infty$) is shown on figure 5, both for the case of no tilt-correction and perfect tilt correction. Spatial filtering clearly reduces the coherence losses.

We now briefly compare not the visibility but the actual number of photons participating in the fringes for both the unfiltered and filtered cases. From figures 3 and 4, we find that the optimum aperture sizes from the point of view of maximising the photon-limited $\widehat{\mathrm{V}^2}$ are respectively $D \simeq 2.3 r_0$ and $D \simeq 3.2 r_0$, both in the case of perfect tilt correction. For these values of the pupil size we can compute the fringe modulation in both cases of $dD/\lambda F = 2$ and $dD/\lambda F \to \infty$ and find $\sqrt{\langle |B_{12}|^2 \rangle} \simeq 2.6$ photon, per incident photon and per $\pi r_0^2/4$ unit of pupil area. It is therefore possible, at least in principle, to increase the measured visibility without reducing the fringe modulation, because larger apertures are allowed when spatial filtering is performed.

At this point, it should be obvious that spatial filtering is a good thing to do when the target is unresolved and the associated wavefronts, would there be no atmosphere, are originally flat. But the reader may be worried of the impact spatial filtering could have on measurements of resolved sources. (S)he might ask, "Won't spatial filtering modify the incoming wavefronts' shape so much as to artificially rectify them, thereby making all visibility measurements very high?" The answer is no, and the reason is simple.

If an interferometer is required to image a particular source, it is because distances comparable to the interferometer baseline are required to resolve the source. This means that the wavefront features arising from the source

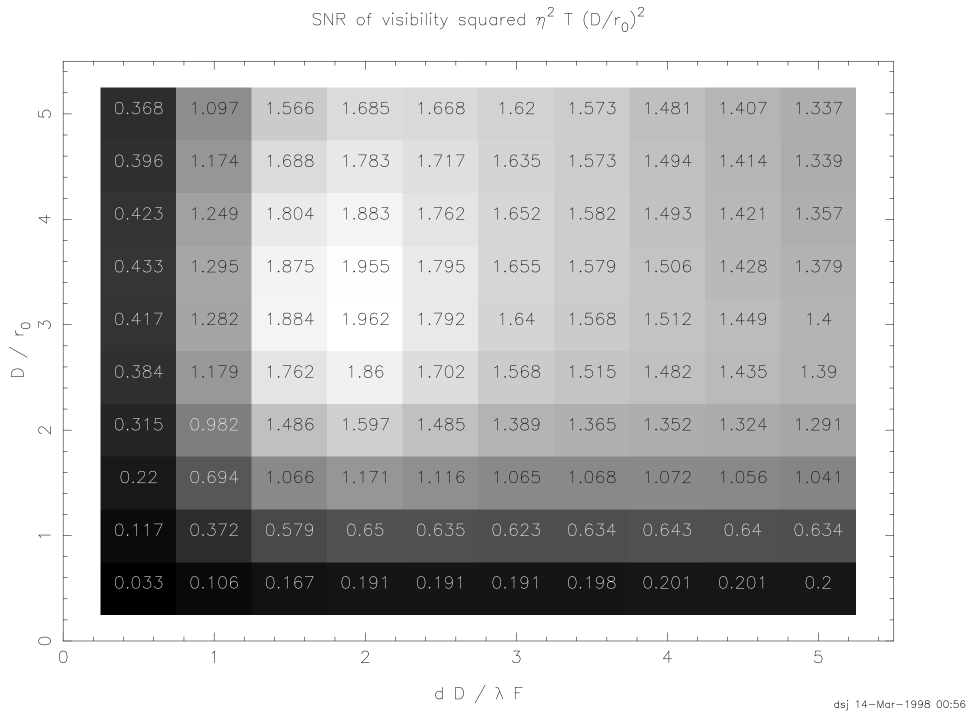

Figure 2. Photon limited signal-to-noise ratio of the visibility squared estimator SNR_{V^2} for a range of value of the normalised parameters D/r_0 and $dD/\lambda F$. Perfect tilt correction is assumed. The results given are per photon, per $\pi r_0^2/4$ unit of telescope pupil area.

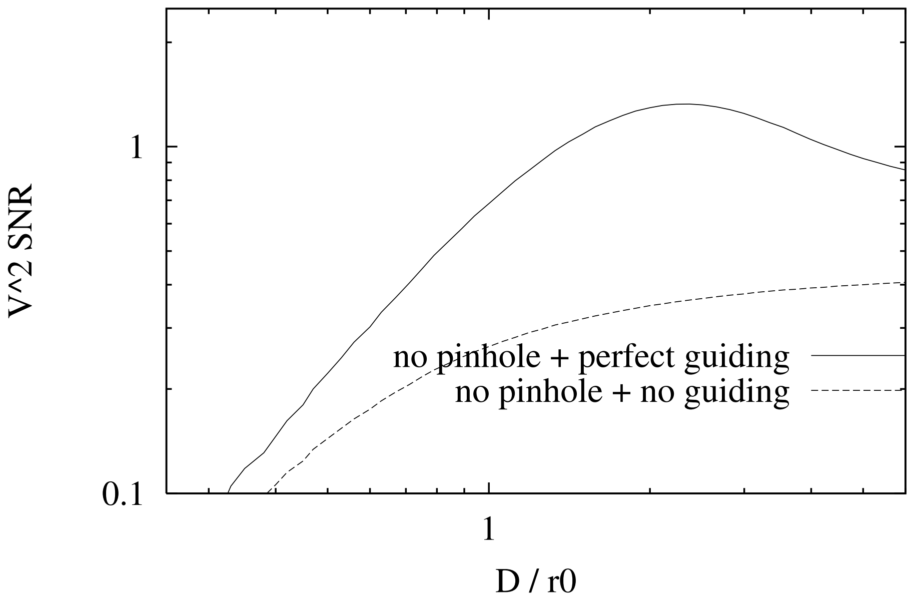

Figure 3. Photon limited signal-to-noise ratio of the visibility squared estimator SNR_{V^2} for a range of seeing conditions, when no pinholes are used. Both cases of no tilt correction and perfect tilt correction are shown.

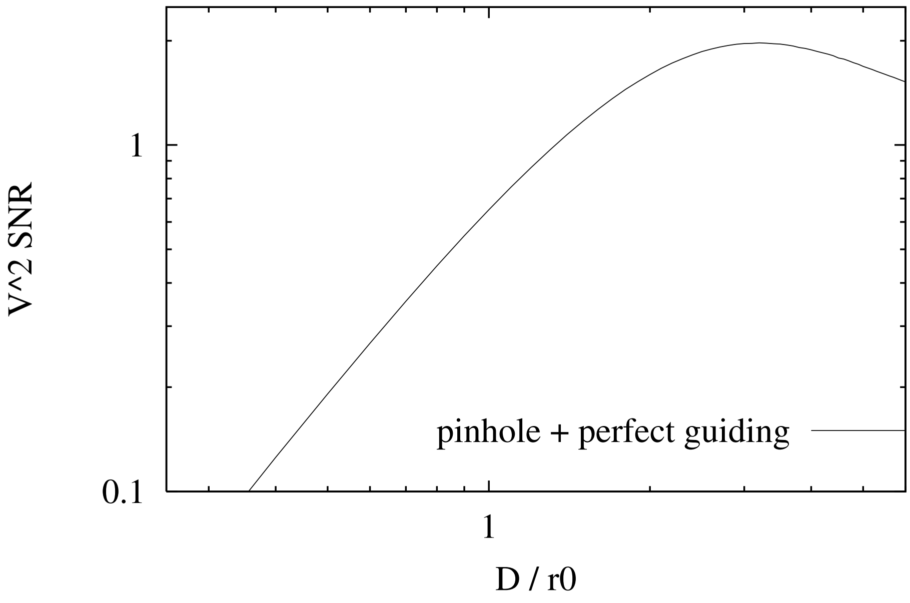

Figure 4. Photon limited signal-to-noise ratio of the visibility squared estimator SNR_{V^2} for a range of seeing conditions and a pinhole of optimum size. Perfect tilt correction is assumed.

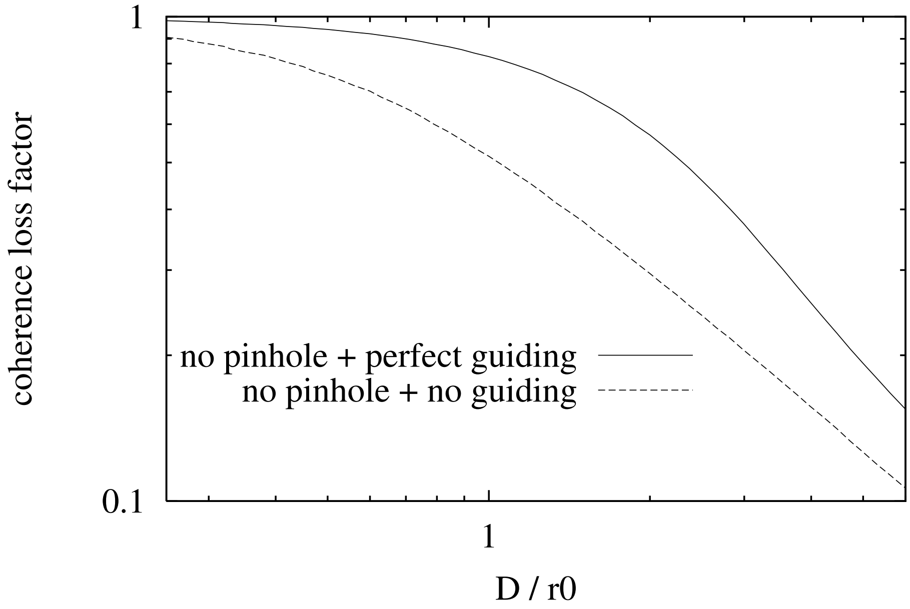

Figure 5. Coherence loss factor η for a range of seeing conditions, when no pinholes are used. Both cases of no tilt correction and perfect tilt correction are shown.

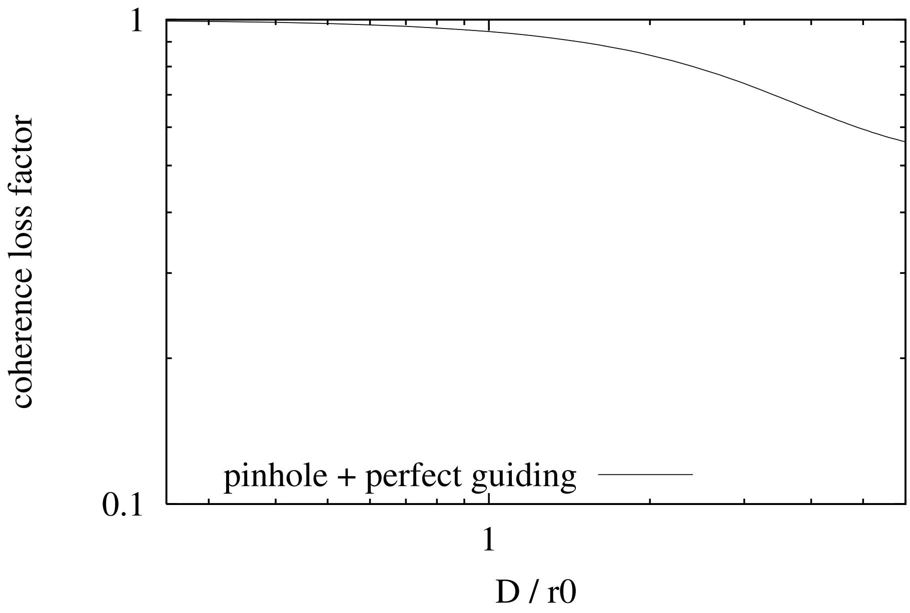

Figure 6. Coherence loss factor η for a range of seeing conditions and a pinhole of optimum size. Perfect tilt correction is assumed.

structure are on the scale of the baseline. Conversely, the interferometer's individual telescopes, much smaller than the baseline, are incapable of resolving the source on their own. In the detector image plane, because of the Fourier Transform performed by the detector lens, these large scale wavefront features will be located very near the optical axis, but convolved and smeared by the wide, low-resolution Airy disc of the small individual telescopes. Therefore, in the absence of atmospheric distortions, in the pinhole plane the difference in size between a resolved and an unresolved source is neglectible. On the other hand, atmospheric distortions of the wavefronts are on scales comparable to the size of the individual telescopes; consequently in the detector image plane these small scale wavefront distortions show as a random halo extending comparatively far away form the optical axis. Practically nothing related to the source is removed when we mask out the halo using a pinhole, even when the source is well resolved – because it is resolved by the baseline, not the individual telescopes.

6. POTENTIAL FOR SELF-CALIBRATED VISIBILITY MEASUREMENTS?

Comparing the coherence loss factor obtained when using a pinhole of optimum size as a spatial filter, shown on figure 6, to the traditional no-pinhole case of figure 5, one notices that the sensitivity to seeing fluctuations is reduced greatly, as indicated by the shallower slope of the pinhole case. This is especially true for the region corresponding to the COAST telescope size and the range of seeing conditions under which COAST operates, typically such that D/r_0 ranges between 2 and 4.

Furthermore, because the pinhole is approximately the size of the beam's diffraction limit, one doesn't expect the instantaneous detector $\vec{\alpha}$–plane image to show features of size much smaller than the pinhole aperture. Therefore, at any given time the pinhole aperture is roughly uniformly illuminated. In these conditions, a pinhole acts more like a single-mode filter than a low-pass filter, because although it lets a range of modes through, they more or less always come in similar proportions.

Practically, this uniform illumination of the pinhole aperture means that when a pinhole is used, spatial wavefront fluctuations are mostly transformed into intensity fluctuations. Indeed, experimentally the signal scintillation increases dramatically when pinholes are used. But this doesn't matter: at any time there is either light or no light through the pinhole, but the light there is, is always "good". This opens the door to the prospect of self-calibrated visibility measurements. Assuming the remaining visibility loss incurred using a pinhole are due only to uniform scintillation across the pinhole aperture, one can write

$$\eta^2 = \left\langle \frac{4I_1(t)I_2(t)}{(I_1(t)+I_2(t))^2} \right\rangle \tag{22}$$

Note that this expression also accounts for any systematic difference in beam brightnesses.

This could be calibrated for in the following way. After acquiring fringes on a particular target, rather than turn to a calibrator star, a time-consuming process which introduces a lot of uncertainty, one acquires some calibration data from both arms independently. This can be done within seconds of acquiring the fringes, rather than several minutes, and seeing conditions won't have changed so much. These observations will of course show no fringes, but severe scintillation: from the probability distribution of intensity $\gamma(I)$ of individual beams, one can infer the coherence loss factor:

$$\eta^2 = \int_{I_1}\int_{I_2} \gamma_1(I_1)\,\gamma_2(I_2)\,\frac{4I_1(t)I_2(t)}{(I_1(t)+I_2(t))^2}\,\frac{(I_1(t)+I_2(t))^2}{\langle(I_1(t)+I_2(t))^2\rangle} dI_1\,dI_2 \tag{23}$$

where the last term accounts for the relative contribution to the COAST $\widehat{\mathrm{V}^2}$ estimator. Recall from equation 7 that this is computed from an average power spectra, and the contribution of a particular fringe realisation to the estimator is in proportion of the squared modulation, i.e. of the square of the product of the visibility and the intensity.

In principle, the probability distribution of the scintillation could even be recovered from the fringe data itself. Because of the way beam combination is done at COAST, there is always a pair of outputs for which the fringes are out of phase by 180°; the sum of these two outputs has no fringes, and twice the scintillation. Note that in this case only an average probability distribution for the two beams can be recovered, and there would still remain to calibrate for systematic differences in beam brightness, but this should not vary in time to much and could be done less frequently, say daily.

7. PRELIMINARY EXPERIMENTAL RESULTS

We have installed a prototype spatial filter set-up similar to that described by figure 1 in one of the outputs of the COAST beam combination optics and used it for preliminary observations on 20 March 1998. The set-up consisted of a $d = 20\ \mu$m pinhole sandwiched between two off-the-shelf achromatic doublet lenses of focal lens $F = 100$ mm. The lenses were stopped down to a diameter of 10 mm, which corresponds to an effective pupil diameter of $D = 160$ mm when the telescope $\times 16$ magnification is taken into account. The experiments were carried out using narrow-band filters specified as $\lambda = 830$ nm, $\delta\lambda = 40$ nm.

The coarse seeing estimate provided by the autoguider was $r_0 \simeq 11$ cm at $\lambda = 830$ nm. Therefore the two dimensionless parameters corresponding to these experiments were approximately

- $D/r_0 \simeq 1.4$;
- $dD/\lambda F \simeq 2.4$ (first null of the Airy disc).

Note that these are not the optimum parameters as we've defined them in section 5.

We have observed two unresolved targets at very different elevations to test the sensitivity of the measurements to variations in seeing conditions. Table 1 summarises the results. The third column is the result form one of the unfiltered "standard" outputs, and the last column is the filtered output. Both the measured coherence η and the SNR of visibility squared measurement $\mathrm{SNR}_{\mathrm{V}^2}$ are given. For both targets, it is clear that using a spatial filter

Table 1. Experimental results testing the sensitivity of η to variations in r_0.

		unfiltered	filtered
α Lyrae	η	0.315	0.552
elev. $\simeq 80°$ (good seeing)	$\mathrm{SNR}_{\mathrm{V}^2}$	2.62	1.69
α Aquilae	η	0.264	0.539
elev. $\simeq 40°$ (poor seeing)	$\mathrm{SNR}_{\mathrm{V}^2}$	0.66	0.48

improves the measured visibility. Comparing the visibility of the two targets, one sees that the filtered measurement is far less sensitive to differences in the seeing conditions. Without a spatial filter, the visibility measured at the two elevations differ by $\simeq 20$ per cent; with a filter, they differ only by $\simeq 2$ per cent.

The $\mathrm{SNR}_{\mathrm{V}^2}$ suffers, but this is not surprising given that we were not operating at the optimum parameters; furthermore this figure of merit is very sensitive to guider performance, which of course in reality is not quite as perfect as what we assumed in the formal treatment above.

We have tried to implement the statistical calibration scheme discussed in section 6. The trend was in the right direction, i.e. there was more scintillation at lower elevation, but the figures didn't quite add up. It is worth noting that eventually, all one needs for the purpose of self-calibration is a strong, well established statistical correlation between scintillation and coherence loss, rather than a formal one-to-one relationship.

8. CONCLUSION

The theoretical investigation we have performed shows that using pinholes as spatial filters can lead to an improvement of up to 50 per cent in the photon limited SNR of visibility squared measurements. This optimum performance is reached for telescopes of size $D \simeq 3.2 r_0$ and pinhole of diameter $d \simeq 82$ per cent of the first null ring of the diffraction-limited Airy disc of the telescope pupil. The SNR of fringe phase measurements, crucial to interferometric imaging of complex sources, is also maximised for these parameters, with the improvement reaching 80 per cent.

For this optimum combination of pupil size, seeing conditions and pinhole size, the coherence loss factor η is reduced by up to a factor of 2. Furthermore, its sensitivity to variations in the seeing conditions $\partial\eta/\partial r_0$ is reduced by up to a factor of 3 for telescope diameters ranging from 2 to 4 r_0.

Spatial filtering permits the rejection of the incoherent, "bad" photons, while keeping most of the coherent, "good" photons. Because slightly larger apertures are allowed, it turns out that the actual number of "good" photons is maintained and the fringe modulation is preserved: it is only the incoherent illumination which is cut down.

Preliminary experiments on unresolved targets have indeed shown improvement in the measured visibility and reduction in seeing sensitivity.

Finally, we have discussed how spatial filtering effectively trades wavefront fluctuations for measurable intensity fluctuations. Better understanding of this process could lead to visibility calibration from the data itself, rather than from data acquired on a nearby calibrator star. This would greatly improve the final error budget on visibility measurements, currently limited by the variations in seeing conditions during the change-over interval between the target and its calibrator.

ACKNOWLEDGMENTS

D. St-J. wishes to thank Corpus Christi College, the Mullard Radio Astronomy Observatory and the Cambridge Philosophical Society for financing his attendance at this conference.

REFERENCES

1. J. W. Goodman, *Introduction to Fourier Optics*, Physical and Quantum Electronics, McGraw-Hill, 1968.
2. J. E. Baldwin, R. C. Boysen, C. A. Haniff, P. R. Lawson, C. Mackay, J. Rogers, D. St-Jacques, P. J. Warner, D. M. A. Wilson, and J. S. Young, "Current status of COAST." These Proceedings.
3. T. J. Pearson and A. C. S. Readhead, "Image formation by self-calibration in radio-astronomy," *Ann. Rev. Astron. Astrophys.* **22**, pp. 97–130, 1984.
4. F. Roddier, "The effects of atmospheric turbulence in optical astronomy," in *Progress in Optics*, E. Wolf, ed., vol. XIX, North-Holland, 1981.
5. D. L. Fried, "Statistics of a geometric representation of wavefront distortions," *J. Opt. Soc. Am.* **55**(11), pp. 1427–1435, 1965.
6. D. L. Fried, "Optical resolution through a randomly inhomogeneous medium for very long and very short exposures," *J. Opt. Soc. Am.* **56**(10), pp. 1372–1379, 1966.
7. M. Teague, "Irradiance moments: their propagation and use for unique retrieval of phase," *J. Opt. Soc. Am.* **72**(9), pp. 1199–1209, 1982.
8. R. J. Noll, "Zernike polynomials and atmospheric turbulence," *J. Opt. Soc. Am.* **66**(3), pp. 207–211, 1976.
9. A. Hewish, "The diffraction of radio waves in passing through a phase-changing ionosphere," *Proc. R. Soc. Lond. A* **209**, pp. 81–96, 1951.
10. S. B. Shaklan, M. M. Colavita, and M. Shao, "Visibility calibration using single mode fibers in a long-baseline interferometer," in *ESO conference on high-resolution imaging by interferometry II, Garching bei München, Germany*, J. M. Beckers and F. Merkle, eds., no. 39 in ESO Conference and Workshop Proceedings Series, pp. 1271–1283, 1992.
11. J. K. Wallace, "Palomar testbed interferometer." These Proceedings.
12. V. Coudé du Foresto, S. Ridgeway, and J.-M. Mariotti, "Deriving object visibilities from interferograms obtained with a fiber stellar interferometer," *Astron. Astrophys. Suppl. Ser.* **121**, pp. 379–392, 1997.
13. V. Coudé du Foresto, G. Perrin, J.-M. Mariotti, M. G. Lacasse, and W. A. Traub, "FLUOR/IOTA stellar interferometer." These Proceedings.
14. S. Prasad and G. Loos, "Spatial filtering of atmospheric decorrelation from wavefronts for interferometry," *Optics Communications* **99**, pp. 380–392, 1993.
15. D. Buscher, "Optimizing a ground-based optical interferometer for sensitivity at low light levels," *Mon. Not. R. astr. Soc.* **235**, pp. 1203–1226, 1988.
16. W. J. Tango and R. Q. Twiss, "Michelson stellar interferometry," in *Progress in Optics*, E. Wolf, ed., vol. XVII, North-Holland, 1980.